Longbottom, R., Fruttiger, M., Douglas, R. H., Martinez-Barbera, J. P., Greenwood, J. & Moss, S. E. (2009). Genetic ablation of retinal pigment epithelial cells reveals the adaptive response of the epithelium and impact on photoreceptors. Proceedings of the National Academy of Sciences of the United States of America (PNAS) ISSN 1091-6490, 106(44), pp. 18728-18733. doi: 10.1073/pnas.0902593106

Author final manuscript published in PNAS (2009) 1066(44), 18728-18733

Genetic ablation of retinal pigment epithelial cells reveals the adaptive response of the epithelium and impact on photoreceptors

Rebecca Longbottom[a,1], Marcus Fruttiger[a,1], Ron H Douglas[2], Juan Pedro Martinez-Barbera[3], John Greenwood[1] and Stephen E Moss[1]

[1]MacTel Laboratory Research Group, Department of Cell Biology, UCL Institute of Ophthalmology, 11-43 Bath Street, London EC1V 9EL, UK.
[2]Henry Wellcome Laboratory for Vision Sciences, Department of Optometry and Visual Science, City University, Northampton Sq, London EC1V 0HB, UK.
[3]Neural Development Unit, Institute of Child Health, 30 Guilford Street, London WC1N 1EH, UK

[a]These authors contributed equally to this work

Author for correspondence:
Professor Stephen E Moss
Department of Cell Biology,
UCL Institute of Ophthalmology,
11-43 Bath Street,
London EC1V 9EL, UK.

Tel: +44 (0)20 7608 6973
Fax: +44 (0)20 7608 4034
Email: s.moss@ucl.ac.uk

Number of text pages: 23

Abstract

The retinal pigment epithelium (RPE) plays a critical role in the maintenance of the outer retina. RPE cell death or dysfunction drives the pathophysiology of many retinal diseases, but the physiological response of the retina to RPE cell loss is poorly understood, mainly because of the absence of suitable experimental models. Here, we generated a transgenic mouse in which an inducible Cre recombinase is expressed exclusively in the RPE under the control of the monocarboxylate transporter 3 gene promoter (RPE^{CreER}). This was crossed with a transgenic mouse harbouring a diphtheria toxin A (DTA) chain gene rendered transcriptionally silent by a floxed stop sequence. We show that activation of DTA in the double transgenic mouse (RPE^{CreER}/DTA) led to 60-80% RPE cell death, with surviving cells maintaining the integrity of the monolayer by increasing their size. Despite the apparent morphological normality of the enlarged RPE cells in the RPE^{CreER}/DTA mice, functional analysis revealed significant deficits on electroretinography, and retinal histopathology showed regions of photoreceptor rosetting and degeneration though with retention of a normal vascular network. Our study reveals that whilst the RPE monolayer has a remarkable intrinsic capacity to cope with cellular attrition, specific aspects of RPE multifunctionality essential for photoreceptor survival are compromised. The RPE^{CreER}/DTA mouse offers advantages over models that employ chemical or mechanical strategies to kill RPE cells, and should be useful for the development and evaluation of RPE-based therapies such as stem cell transplantation.

\body

Introduction

The retinal pigment epithelium (RPE) is a monolayer of multifunctional epithelial cells that physically abuts the photoreceptor layer and effectively forms the posterior blood-retinal barrier. RPE cells contain photoprotective pigment granules, phagocytose shed photoreceptor outer segments (POS), recycle 11-cis retinal, and regulate ion and nutrient fluxes between the outer retina and choriocapillaris (1). Defects in any of these essential activities may cause secondary photoreceptor dysfunction, retinal degeneration and blindness. For example, humans and rodents that lack the Mer tyrosine kinase exhibit severely defective phagocytosis of POS and undergo rapid retinal degeneration (2, 3), and mutation or loss of RPE65 in patients with Leber's Congenital Amaurosis leads to failure of the visual cycle and progressive retinal degeneration (4, 5). Although these are relatively rare conditions, the many energy-dependent activities of RPE cells create a metabolic burden in normal individuals that increases with age, and which is manifest in the accumulation of insoluble waste products such as the toxic bis-retinoid lipofuscin (6). In humans this leads to a decrease in RPE cell numbers with age (7, 8), whereas age-related photoreceptor loss appears to correlate more specifically with lipofuscin levels in the underlying RPE (9).

Various experimental models have been used to investigate the effects on the retina of RPE loss, stress or dysfunction. The principle methods used to kill RPE cells have been chemical ablation using sodium iodate, and mechanical debridement to physically remove the RPE. Several distinct responses to sodium iodate have been reported, including loss of adhesion between the retina and RPE (10), photoreceptor degeneration (11) and atrophy of the choriocapillaris (12). Some of these features have also been reported following surgical debridement of the RPE, for example, pathological changes to the choriocapillaris in rabbits and cats (13-15). Photoreceptor degeneration following loss of RPE occurs regardless of method used, but RPE re-growth has been noted only following debridement in pig eyes (16). Both

experimental strategies achieve RPE loss, but may also induce off-target effects or indirect responses such as inflammation following necrotic cell death (11). RPE proliferation observed upon debridement most likely occurs as a consequence of the procedural retinal detachment, as in proliferative vitreoretinopathy, where loss of the intimate physical association with the photoreceptors permits RPE cells, even while contact inhibited, to enter the cell cycle (17, 18).

To circumvent these problems, we have developed a mouse model in which conditional genetic ablation of the RPE leads to a rapid and profound reduction in RPE cell number. We find that the RPE monolayer is highly adaptive in its ability to compensate for significant individual cell loss, maintaining an effective blood-retinal barrier and normal monolayer thickness in the absence of significant cell division. However, other RPE-dependent activities necessary for normal photoreceptor function are impaired leading to anatomical and functional changes in the retina. Our model provides new insight into the relationship between RPE cells and retina, and should be useful for studies aimed at repopulating or replacing RPE following death or dysfunction in disease.

Results

Cre Recombination Activity in RPE^{CreER} Mice. In order to genetically target the RPE we made transgenic mice that express a tamoxifen-inducible form of Cre recombinase (iCreER^{T2}) (19-21) under the transcriptional control of a gene that is specifically expressed in the RPE. It has been previously shown that the monocarboxylate transporter 3 (Mct3, also known as Slc16a8) is only expressed in two cell populations, RPE in the eye and choroid plexus epithelium in the brain (22, 23). We therefore obtained a bacterial artificial chromosome (BAC) containing the Mct3 gene, placed the coding sequence for iCreER^{T2} into its open reading frame (Fig. 1*A*) using homologous recombination in *E. coli* (24) and used it to make transgenic mice by pronuclear injection. The BAC contained about 114kb genomic sequence upstream and about 59kb downstream of the Mct3 gene and, due to its large size, is likely to contain all the regulatory elements required to replicate endogenous Mct3 expression.

Cre recombination activity in the resulting mouse strain was tested in a ROSA-lacZ reporter background (25). In this reporter strain a loxP-flanked stop cassette normally prevents the expression of lacZ, but upon Cre activation via systemic tamoxifen delivery, the stop cassette is removed and lacZ is expressed, reporting Cre recombination activity. In the first instance, we induced newborn RPE^{CreER} x ROSA-lacZ mice with a single injection of 4-hydroxytamoxifen (the metabolically active form of tamoxifen). After one week lacZ expression was assessed in sclera/RPE whole mounts. We found strong staining in a subpopulation (approximately 20%) of RPE cells in mice containing the iCreER^{T2} transgene but not in iCreER^{T2}-negative littermates (Fig. 1*B*). We also observed lacZ expression in choroid plexus epithelium in the brain (Fig. 1*C*), confirming Mct3 specific expression of the transgene. We then induced Cre activity in adult mice (6 weeks old) because an adult experimental paradigm is more relevant for human RPE dysfunction, which typically displays adult onset. Two weeks after tamoxifen administration we found that recombination had occurred in approximately 5% of RPE cells, revealing lower recombination efficiency in adult than in neonatal animals (Fig. 1*D*). Cross

sections demonstrated that recombination activity was restricted to the RPE and completely absent from the retina (Fig. 1*E*).

Genetic Ablation of the RPE. In order to recreate certain aspects of RPE pathology in human eye diseases we utilised the RPE^{CreER} mice to genetically ablate RPE cells. To this end we generated RPE^{CreER}/DTA mice by crossing the RPE^{CreER} strain with mice that conditionally express diphtheria toxin A chain (DTA) under a ubiquitous promoter (26) (Fig. 2*A*). In this and all subsequent experiments tamoxifen was administered to adult animals (see Supplementary Table 1 for details of ages). After tamoxifen administration we used an antibody against ZO-1 (visualising tight junctions and the outline of RPE cells) to assess changes in the RPE. Six days after tamoxifen administration numerous individual RPE cells became rounded, lost their well defined ZO-1 staining and were extruded towards the retina (Fig. 2*B*). Two weeks after tamoxifen application the remaining RPE cells appeared enlarged and irregular in shape with clumps of extruded cells in the subretinal space (Fig. 2*C-D* and Fig. S1). In comparison to the ROSA-LacZ background the percentage of affected cells was significantly higher in the ROSA-DTA background with an average 68% reduction of RPE cell numbers after 14 days (Fig. 2*E*). However, after the initial wave of RPE loss cell numbers stabilized and remained unchanged between 14 days and 6 months (Fig. S2). RPE flat mounts from animals 2 weeks post tamoxifen and wild type littermates revealed that dead cells did not leave gaps in the continuity of the epithelium. Instead, surrounding cells dramatically increased their size to prevent holes appearing (Fig. 2*F*). The RPE^{CreER}/DTA cells were found to be more irregularly shaped (Fig. 2*G*) with significantly longer perimeters (Fig. 2*H*), and a significant reduction in the total length of junctional interfaces between cells, measured by assessing the perimeter:area ratio (Fig 2*I*). The impact on cell-cell junctions was also investigated by western blotting protein fractions isolated from the RPE cells of both RPE^{CreER}/DTA and wild type control eyes (Fig. 2*J*). An average 42% reduction in the amount of ZO-1 was observed (Fig. 2*K*) ($p < 0.001$), which

corresponds to the reduction in the 43% perimeter:area ratio calculated from the RPE flat mount analysis (Fig. 2*I*). In addition, there were significant reductions in the relative levels of RPE65 and MerTK in the tamoxifen-treated animals (Fig. 2*L-O*) suggesting possible deficits in the visual cycle and phagocytosis respectively, two aspects of RPE cell function vital for photoreceptor survival.

Ultrastructural Changes in Surviving RPE Cells. Since the average diameter of surviving RPE cells was significantly increased, we tested whether the cell spreading was associated with a reduction in cell thickness. Electron microscopy (EM) was performed on wild type (Fig. 3*A*) and RPE^{CreER}/DTA (Fig. 3*B*) retinas to measure the thickness of the RPE cells. Surprisingly, there was no difference in RPE cell thickness (Fig. 3*C*) indicating that the fold-increase in cell 'footprint' corresponds directly to an increase in cell volume. One of the functions of the RPE cell is to phagocytose shed photoreceptor outer segments. The EM images of the retinas allowed us to quantify the number of phagosomes per unit length of RPE (Fig. 3*D*) and the cellular localisation (apical versus basal) of phagosomes (Fig. 3*E*). The cellular localisation gives an insight into phagosome processing and thus provides an indication of the functionality of the RPE cell. Despite the reduced level of MerTK expression (Fig. 2*N*), there was no significant difference in the number of phagosomes per unit length of RPE. However, there was an increase in the proportion of phagosomes in the basal half of the RPE cells in the RPE^{CreER}/DTA retinas when compared to wild type littermate controls, suggesting that phagolysosomal fusion and processing may be defective in these animals.

Morphological Changes in the Retina. Semi-thin sections and immunohistochemical techniques were used to assess the retinal morphology of the RPE^{CreER}/DTA mice. These analyses revealed varying degrees of morphological abnormality in the RPE^{CreER}/DTA mice, the major change being the appearance of retinal folds termed rosetting. The extent of rosetting

varied between animals, with some severely (Fig. 3*H*) and some mildly affected (Fig. 3*G*) in comparison to a wild type (Fig. 3*F*) retina. We also immunostained sections of retina using protein markers whose expression lies both within and outside the areas that are morphologically altered in the RPE^{CreER}/DTA retinas. Phalloidin was used to visualise the F-actin distribution throughout all the layers of the retina (Fig. S3*A*-*B*). The distribution of F-actin, though altered at the anatomical level, was consistent at the cellular level with the pattern of F-actin expression in wild type retinas. Thus, regions of enrichment are still aligned with the same cellular boundaries, principally flanking the photoreceptor inner segments. PKCa (Fig. S3*C*), cone transducin (Fig. S3*D*), and mGluR6 staining were unaffected in the RPE^{CreER}/DTA retinas (Fig. S3*E*). There was however a change in the expression of Müller cell glial fibrillary acidic protein (GFAP), with an increase in staining in the inner plexiform and inner nuclear layers of the retina (Fig. S3*F*), consistent with retinal stress (27). We also observed staining for macrophages/microglia in the RPE^{CreER}/DTA retinas especially in the subretinal space and outer retina (Fig. S3*G*). This, however, did not correlate with the appearance of deep leakage (Fig. S3*H*) and indicates that RPE barrier function is maintained even during significant cell loss. Histological assessment of the retinas of the RPE^{CreER}/DTA mice at 6 months revealed no vascular anomalies despite clear alterations to the RPE and outer nuclear layer, and a normal vascular network in the RPE^{CreER}/DTA mice was confirmed in retinal flat mounts (Fig. S4).

RPE Stress Reduces Visual Function. To assess the effects of RPE cell death on photoreceptors, we measured rhodopsin levels and investigated visual function in RPE^{CreER}/DTA mice two weeks following tamoxifen induction. Rhodopsin levels were measured by spectral analysis of pre- and post-bleach visual pigment absorbance, which revealed no significant difference in the amount of pigment extracted from the RPE^{CreER}/DTA animals in comparison to control animals (Fig. 4). Electroretinography (ERG) was used to assess the functional responsiveness of the neural retina of the RPE^{CreER}/DTA mice, using full-field flash stimuli under

scotopic and photopic conditions. Representative traces from wild type (Fig. 5*A* and *D*) and RPE^{CreER}/DTA mice (Fig. 5*B*, *E* (1 animal) and Fig. 5*C*, *F* (1 animal)) illustrate the range of responses observed following RPE cell ablation. Under scotopic conditions the ERG responses are principally produced by the rods, which in the RPE^{CreER}/DTA mice revealed significantly reduced a wave ($p < 0.011$) and b wave ($p < 0.005$) amplitudes in comparison to wild type controls (Fig. 5 *G-H*). After a period of light adaption, cone function was assessed under photopic conditions (Fig. 5*I*) but there was no significant difference in the b wave amplitudes in the two experimental groups. At the highest light intensity tested scotopically, log intensity 1, the initial a wave slope, which was taken within the first 10 ms of the ERG response, was significantly reduced in the RPE^{CreER}/DTA animals (Fig. 5*J*). These changes in ERG amplitudes were neither a transient response to RPE cell loss nor a prelude to further decline, remaining stable for at least a further 6 months (Fig. S5). Scotopic responses from the wild type animals were of comparable amplitudes to those previously reported in C57B/6 animals (28). The reduction in scotopic amplitude and a wave gradient indicate that the functionality of the rod photoreceptors is compromised, though in many animals this was in the absence of any detectable histological changes within the retina and normal levels of visual pigment.

Discussion

In this study we report the development of a transgenic mouse in which inducible expression of the DTA gene was used to specifically kill RPE cells. Cell type-specific targeting of the transgene was achieved by integration of the Cre recombinase into a BAC containing the Mct3 gene, a proton-coupled monocarboxylate transporter, which in the eye is expressed uniquely in the RPE (22, 29). Activation of DTA led to a phase of cell death lasting a few days, during which individual dying cells appeared to be extruded from the monolayer with concomitant enlargement of the surrounding cells. The behaviour of the RPE *in vivo* is therefore consistent with that observed in studies on epithelial monolayers in culture, in which cells primed for apoptosis undergo an actin and myosin dependent 'purse-string' expulsion (30). Such a mechanism would explain the appearance in certain retinal sections of clumps of pigmented cells at the RPE/photoreceptor interface, though since RPE cells are inherently phagocytic it is also likely that some of the dead cells were ingested both by their surviving neighbours as well as invading macrophages.

A key question in diseases such as AMD, in which RPE cell death or dysfunction leads to secondary photoreceptor degeneration (31), is whether or not the surviving RPE cells have any capacity for self-renewal that might be stimulated to therapeutic benefit. A subsidiary issue is whether, if the intrinsic barriers to RPE cell proliferation can be overcome, problems may be encountered in re-populating an age-modified Bruch's membrane that has been shown to be hostile both to cell attachment *in vitro* (32, 33) and to autologous RPE *in vivo* following surgical translocation (34, 35). In the RPE^{CreER}/DTA mice, RPE cell death is induced in a healthy retina in which we assume Bruch's membrane offers a favourable substrate for cell growth, yet in both newborns and adults there was no evidence of cell proliferation as judged by incorporation of BrdU or phosphohistone staining (not shown). Indeed a striking feature of the cell-depleted RPE monolayer was the increase in 'footprint' of the surviving cells, in which the largest cells expanded to almost 20 times their normal size. Increases in RPE cell size and irregularity have

also been observed in the retinas of patients with AMD (36), particularly in association with Drusen, thus the RPE^{CreER}/DTA mice may to some extent recapitulate the pigment epithelial cell response in AMD. These data are also consistent with the idea that in geographic atrophy the exposed extracellular matrix is prohibitive to RPE cell attachment and/or survival as it is unable to accommodate RPE cell expansion from the surrounding population.

Despite maintaining a functionally intact monolayer, RPE cell function was clearly compromised. Several animals exhibited rosetting or retinal folds, a characteristic of several human retinal diseases that has also been described in various models of retinal degeneration. Although the mechanisms that drive rosette formation are not understood, it may occur as a consequence of a loss of close interdigitation between the RPE and outer segments. We also observed deficits in scotopic ERG a and b wave amplitude in RPE-depleted animals, irrespective of the presence or absence of retinal structural abnormalities. This suggests that even in anatomically normal photoreceptors, changes in the depleted epithelial monolayer influence phototransduction. This could occur through alterations in ion and electrolyte flow between the RPE and retina, or possibly through disruption to the visual cycle. In addition, retrieval of photopigment from phagocytosed outer segments may be compromised in the RPE^{CreER}/DTA mice given the accumulation of phagosomes in the basal RPE. This is suggestive of a delay in phagolysosomal fusion and is consistent with defects in phagosome motility reported in a model of sub-lethal photic RPE stress (37).

In summary, we have shown that although the RPE can accommodate a significant level of cell loss, at least with regard to maintaining a confluent and intact monolayer, it is unable to fully support the functional demands of the outer retina. Thus in aged humans, loss of RPE may place an excessive burden on the remaining population and hence predisposition to retinal dysfunction in the area of greatest metabolic demand.

Materials and Methods

Generation of RPE^{CreER}/DTA Mice and Tamoxifen Administration. A plasmid coding for iCreER^{T2}-IRES-EGFP-pA and a FRT flanked kanamycin resistance cassette (19) was used for recombinant targeting of a BAC containing the Mct3 gene, Slc16a8 (RP24-149-K18, provided by the UK HGMP Resource Centre). The 5' and 3' homologies for recombinant targeting were created by PCR amplification from the same BAC and cloned into the targeting plasmid. The iCreER^{T2}-IRES-EGFP-pA sequence was placed at the start of the open reading frame of the Mct3 gene (removing exon 3) in the BAC by homologous recombination in EL250 bacteria (24) (kindly provided by N. Copeland) using the kanamycin resistance cassette to screen for clones that have undergone recombination. The resistance cassette was then removed by arabinose-induced Flp recombinase activity in EL250 bacteria (24). The resulting BAC was purified and used for mouse transgenesis in a C57Bl6 X CBA F2 background as described (38). Offspring were genotyped using PCR with the primers 5'-GGGTGTCCTGGGCTGTTTCTCTTT-3' and 5'-CTCCCCAGCATCCACATTCTCCTT-3'. Heterozygous, male RPE^{Cre} animals were then crossed with homozygous female conditional DTA animals (26) resulting in offspring that contained a conditional DTA allele in 100% and the Cre allele in 50% of the pups. OHT was administered via intraperitoneal injection (20 µg per newborn pup) and tamoxifen via gavage (3 mg per adult, 2-5 months old). *In vivo* tamoxifen is converted to OHT which is the biologically active form of tamoxifen.

Histology. For X-gal staining tissue was dissected and fixed in 0.2% glutaraldehyde, 2 mM $MgCl_2$, 5 mM EGTA in PBS for 30 min at room temperature. Following incubation in wash buffer (PBS containing 5 mM EGTA, 0.01% sodium deoxycholate and 0.02% Nonidet P-40) tissue was incubated in wash buffer also containing 5 mM $K_3Fe(CN)_6$, 5 mM $K_4Fe(CN)_6$ and 1 mg/ml X-gal overnight at 37°C. In order to better visualise X-gal staining in the RPE, pigment was bleached

(after X-gal staining) by incubation in $KMnO_4$ (0.25% in water) for 10 min at room temperature and subsequent incubation in oxalic acid (1% in water) for 20 min at room temperature.

Retinal whole mount preparations were dissected from whole eyes after brief fixation in 2% (w/v) paraformaldehyde in PBS and then processed for immunohistochemistry as previously described (39). RPE whole mount preparations were dissected from unfixed eyes and then fixed in cold (-20°C) methanol for at least 30 min. Cryo-sections were blocked with 0.1% BSA, 2% goat serum and 0.1% Triton-X in PBS for 10 min and incubated with primary antibodies diluted in the blocking solution for 2 h at room temperature or overnight at 4°C.

RPE flat mount morphological analysis was performed in Metamorph analysis software (Molecular Devices, USA) from images of flat mounted eye cups where the neuroretina layers had been removed leaving the RPE cell layer exposed. RPE cells were stained with a rabbit antibody against ZO-1 (Invitrogen, 1:100) and Hoechst 33342, and images captured on an Olympus Axiovert microscope. The perimeters of 150 cells (3 different images) from each eye were traced, and the area, perimeter and shape factor ($4\pi A/P^2$ (A=area, P=perimeter)) were calculated. The closer to 1, the more circular/regular the cell. In the same 3 images, the numbers of cells in a standard ROI were counted, to give an average number of cells within a set reference area for each animal. In total, 6 wild type (WT) animals and 6 transgenic animals (TG) from 3 different litters were analysed 2 weeks post tamoxifen dose. Student's t test was performed for each morphological property analysed.

Vascular endothelial cells were stained using FITC-conjugated isolectin B4 (Sigma, 1:50). Pericytes/smooth muscle cells were stained with a Cy3-conjugated monoclonal anti-ASMA antibody (Sigma, 1:100). Secondary Alexa-488 and Alexa-546 antibodies (Molecular Probes, 1:500) were applied to the sections for 1 h at RT and the sections were mounted in ProLong

Gold anti fade reagent containing DAPI (Molecular Probes) and analysed by fluorescence microscopy.

Western Blotting. RPE protein fractions were isolated in SDS-PAGE sample buffer, resolved by 6% SDS-PAGE and transferred to nitrocellulose membranes. Membranes were washed in Amido black (BD staining solution for 2 min), then washed in destain solution (10% methanol, 10% acetic acid). A loading control image was taken at this stage in PBS. Membranes were further washed in PBS and then blocked and incubated overnight in primary antibodies to ZO1 (gift of Prof. K. Matter), MerTK (R&D Systems) and RPE65 (Chemicon International). HRP conjugated secondary (DAKO) and ECL reagent (Amersham Biosciences) was used for visualisation. Analysis was performed in Metamorph imaging software.

Ultrastructure Analysis. Eyes from 6 WT and 6 TG mice were emersion-fixed and prepared for transmission electron microscopy. Ultra thin sections were viewed on a JEOL 1010 transmission electron microscope and images captured using Gatan Micrograph software and an Orius™ camera. RPE cell thickness and phagosome number and cellular localisation were analysed in imageJ 1.41 software (NIH, USA). The thickness of the RPE was averaged for each animal from measurements made from 5-8 EM images. The averages for all the animals were then included in the statistical analysis by Student's t test. Phagosomes were counted per length of RPE and relative cellular localisation analysis was carried out from the same 5-8 EM images.

Electroretinography. Twelve transgenic (TG) and eleven wild type (WT) mice from six different litters were dark-adapted overnight before ERG on the left eye 2 weeks post tamoxifen. Animals were anaesthetised by Ketamine/Domitor (0.75 ml Ketamine, 0.5 ml Dormitor, 0.75 ml sterile water at 0.2 ml/100g, i.p. supplemented as required). Under red-light conditions, pupils were dilated with topical atropine and phenylephrine. ERG recordings were carried out via platinum

loop electrodes placed on the cornea and a reference platinum electrode in the scalp of the animal. A platinum earth electrode was place subcutaneously on the lower back of the animal. The animal was placed on a heated pad (37°C) in a light-tight box for the recordings. Flash stimuli (3 µs -1 ms duration, repetition rate 0.17 - 0.67 Hz) were presented via an LED stimulator, log intensity -5.5 to +1, under scotopic conditions. After scotopic testing was completed, animals were light-adapted to 20 cd/m^2 background for 20 min. Following light adaption photopic responses to flash stimuli (1 ms – 3 ms duration, repetition rate 0.5 Hz), log intensities -1.4 to +2 and flicker stimuli (up to 40 Hz) were measured. Statistical analysis using specialised software, SPSS, where an analysis of general linear means was performed examined the trends within the populations.

Quantitation of Rhodopsin. TG (n=5) and WT control (n=6) animals were placed in darkness overnight and all subsequent procedures performed under dim red light. They were sacrificed by cervical dislocation and visual pigments were extracted by homogenising whole individual eyes in 0.5 ml PBS and 100 µl of 200 mM n-dodecyl-o-β-l-maltoside. Homogenates were rotated for 2 h at room temperature followed by 10 min centrifugation (4°C, 23,000 x g). The resulting supernatant was scanned (300-700 nm) in a quartz cuvette using a Shimadzu UV-2101 PC spectrophotometer. After the initial scan of the unbleached extract it was exposed to white light for 3 min and rescanned. The maximum absorbance of the difference spectra obtained by subtracting these 2 spectra indicated the total amount of photolabile pigment extracted. The maximum absorbances of the extracts from the 2 eyes of each animal were averaged. The average amounts for each animal were used for statistical analysis by Student's t test.

ACKNOWLEDGMENTS

This study was funded by the Lowy Medical Research Institute Ltd. (The Macular Telangiectasia Project, www.mactelresearch.com) and a programme grant from the Wellcome Trust (ref: GR072694MF). The authors are grateful to Peter Munro and Matthew Pearson for technical assistance.

References

1. Strauss O (2005) The retinal pigment epithelium in visual function. *Physiol Rev* 85:845-881.
2. D'Cruz PM, *et al*. (2000) Mutation of the receptor tyrosine kinase gene Mertk in the retinal dystrophic RCS rat. *Hum Mol Genet* 9:645-651.
3. Gal A, *et al.* (2000) Mutations in MERTK, the human orthologue of the RCS rat retinal dystrophy gene, cause retinitis pigmentosa. *Nat Genet* 26:270-271.
4. Gu SM, *et al*. (1997) Mutations in RPE65 cause autosomal recessive childhood-onset severe retinal dystrophy. *Nat Genet* 17:194-197.
5. Hanein S, *et al*. (2004) Leber congenital amaurosis: comprehensive survey of the genetic heterogeneity, refinement of the clinical definition, and genotype-phenotype correlations as a strategy for molecular diagnosis. *Hum Mutat* 23:306-317.
6. Sparrow JR, Boulton M (2005) RPE lipofuscin and its role in retinal pathobiology. *Exp Eye Res* 80:595-606.
7. Gao H, Hollyfield JG (1992) Aging of the human retina. Differential loss of neurons and retinal pigment epithelial cells. *Invest Ophthalmol Vis Sci* 33:1-17.
8. Del Priore LV, Kuo YH, Tezel TH (2002) Age-related changes in human RPE cell density and apoptosis proportion in situ. *Invest Ophthalmol Vis Sci* 43:3312-3318.
9. Dorey CK, Wu G, Ebenstein D, Garsd A, Weiter JJ (1989) Cell loss in the aging retina. Relationship to lipofuscin accumulation and macular degeneration. *Invest Ophthalmol Vis Sci* 30:1691-1699.
10. Ashburn FS Jr, Pilkerton AR, Rao NA, Marak GE (1980) The effects of iodate and iodoacetate on the retinal adhesion. *Invest Ophthalmol Vis Sci* 19:1427-1432.
11. Kiuchi K, Yoshizawa K, Shikata N, Moriguchi K, Tsubura A (2002) Morphologic characteristics of retinal degeneration induced by sodium iodate in mice. *Curr Eye Res* 25:373-379.

12. Korte GE, Reppucci V, Henkind P (1984) RPE destruction causes choriocapillary atrophy. *Invest Ophthalmol Vis Sci* 25:1135-1145.

13. Leonard DS, Zhang XG, Panozzo G, Sugino IK, Zarbin MA (1997) Clinicopathologic correlation of localized retinal pigment epithelium debridement. *Invest Ophthalmol Vis Sci* 38:1094-1109.

14. Hayashi A, *et al*. (1999) Surgically induced degeneration and regeneration of the choriocapillaris in rabbit. *Graefes Arch Clin Exp Ophthalmol* 237:668-677.

15. Ivert L, Kong J, Gouras P (2003) Changes in the choroidal circulation of rabbit following RPE removal. *Graefes Arch Clin Exp Ophthalmol* 241:656-666.

16. Del Priore LV, *et al*. (1995) Débridement of the pig retinal pigment epithelium in vivo. *Arch Ophthalmol* 113:939-944.

17. Anderson DH, Stern WH, Fisher SK, Erickson PA, Borgula GA (1981) The onset of pigment epithelial proliferation after retinal detachment. *Invest Ophthalmol Vis Sci* 21:10-16.

18. Fisher SK, Erickson PA, Lewis GP, Anderson DH (1991) Intraretinal proliferation induced by retinal detachment. *Invest Ophthalmol Vis Sci* 32:1739-1748.

19. Claxton S, *et al*. (2008) Efficient, inducible Cre-recombinase activation in vascular endothelium. *Genesis* 46:74-80.

20. Feil R, Wagner J, Metzger D, Chambon P (1997) Regulation of Cre recombinase activity by mutated estrogen receptor ligand-binding domains. *Biochem Biophys Res Commun* 237:752-757.

21. Shimshek DR, *et al*. (2002) Codon-improved Cre recombinase (iCre) expression in the mouse. *Genesis* 32:19-26.

22. Philp NJ, Yoon H, Grollman EF (1998) Monocarboxylate transporter MCT1 is located in the apical membrane and MCT3 in the basal membrane of rat RPE. *Am J Physiol* 274:R1824-1828.

23. Philp NJ, Yoon H, Lombardi L (2001) Mouse MCT3 gene is expressed preferentially in retinal pigment and choroid plexus epithelia. *Am J Physiol Cell Physiol* 280:C1319-C1326.

24. Yu D, *et al.* (2000) An efficient recombination system for chromosome engineering in Escherichia coli. *Proc Natl Acad Sci USA* 97:5978-5983.

25. Soriano P (1999) Generalized lacZ expression with the ROSA26 Cre reporter strain. *Nat Genet* 21:70-71.

26. Ivanova A, *et al*. (2005) In vivo genetic ablation by Cre-mediated expression of diphtheria toxin fragment A. *Genesis* 43:129-135.

27. Lewis GP, Fisher SK (2003) Up-regulation of glial fibrillary acidic protein in response to retinal injury: its potential role in glial remodeling and a comparison to vimentin expression. *Int Rev Cytol* 230:263-290.

28. Gresh J, Goletz PW, Crouch RK, Rohrer B (2003) Structure-function analysis of rods and cones in juvenile, adult, and aged C57bl/6 and Balb/c mice. *Vis Neurosci* 20:211-220.

29. Bergersen L, *et al*. (1999) Cellular and subcellular expression of monocarboxylate transporters in the pigment epithelium and retina of the rat. *Neuroscience* 90:319-331.

30. Rosenblatt J, Raff MC, Cramer LP (2001) An epithelial cell destined for apoptosis signals its neighbors to extrude it by an actin- and myosin-dependent mechanism. *Curr Biol* 11:1847-1857.

31. Nowak JZ (2006) Age-related macular degeneration (AMD): pathogenesis and therapy. *Pharmacol Rep* 58:353-363.

32. Tezel TH, Del Priore LV, Kaplan HJ (2004) Reengineering of aged Bruch's membrane to enhance retinal pigment epithelium repopulation. *Invest Ophthalmol Vis Sci* 45:3337-3348.

33. Gullapalli VK, Sugino IK, Van Patten Y, Shah S, Zarbin MA (2005) Impaired RPE survival on aged submacular human Bruch's membrane. *Exp Eye Res* 80:235-248.

34. Cahill MT, Mruthyunjaya P, Bowes Rickman C, Toth CA (2005) Recurrence of retinal pigment epithelial changes after macular translocation with 360 degrees peripheral retinectomy for geographic atrophy. *Arch Ophthalmol* 123:935-938.

35. MacLaren RE, Aylward GW (2005) Delayed atrophy of the retinal pigment epithelium after submacular surgery. *Eur J Ophthalmol* 15:170-172.

36. Al-Hussaini H, Schneiders M, Lundh P, Jeffery G (2009) Drusen are associated with local and distant disruptions to human retinal pigment epithelium cells. *Exp Eye Res* 88:610-612.

37. Burke JM, Zareba M (2009) Sub-lethal photic stress and the motility of RPE phagosomes and melanosomes. *Invest Ophthalmol Vis Sci* 50:1940-1947.

38. Fogarty M, Richardson WD, Kessaris N (2005) A subset of oligodendrocytes generated from radial glia in the dorsal spinal cord. *Development* 132:1951-1959.

39. West H, Richardson WD, Fruttiger M (2005) Stabilization of the retinal vascular network by reciprocal feedback between blood vessels and astrocytes. *Development* 132:1855-1862.

Figure Legends

Fig. 1. Generation and testing of RPE-specific CreER mice. (*A*) Schematic representation of the construction of the BAC incorporating the CreER^{T2} under the expression control of the Mct3 gene. (*B*) RPE/Sclera from neonate animals with the CreER Lac Z transgene (bottom left) showed approximately 20% of the RPE cells were positive, and an absence of any positive X-gal dye in non-transgene animals (top right). (*C*) Similarly, a population of X-gal positive cells was found in choroid plexus epithelium of CreER Lac Z transgenics (left) compared to controls (right). (*D*) Induction of Cre-recombinase activity in adult animals (6 weeks old) was less pronounced. The pigment of the RPE cells has been bleached to enable visualisation of the X-gal dye product. (*E*) A cryosection (20 μm) cut transversely from a Lac Z-Mct3-Cre retina, incubated with X-gal dye, demonstrates the expression of the Lac Z specifically within the RPE cells. RGC-retinal ganglion cells, INL inner nuclear layer, ONL outer nuclear layer, PR photoreceptor layer, RPE retinal pigment epithelium. Scale bars in B, C are 500μm and in D, E 100μm.

Fig. 2. RPE flatmount morphological analysis. (*A*) The cross of Mct3-CreER^{T2} and the ROSA-DTA-loxP cross animals schematic is shown. RPE flat mounts stained with DAPI (Blue) and ZO-1 (green) from animals expressing the DTA 1 week (*B*) and 2 weeks (*C* (WT), *D* (TG)) post tamoxifen administration. The insets (*C*, *D*) show a higher magnification of the area in the co-responding white rectangle, allowing better visualization of the change in morphology of the RPE cells in the transgenic (TG) animals. Morphometric analysis revealed, in the transgenic animals, a significant decrease in the number of cells per unit area (*E,* $p<0.000005$), an increase in cell size (*F,* $p<0.0018$), a reduction in shape factor (*G,* $p<0.000001$), an increase in average cell perimeter (*H,* $p<0.0002$) and a reduction in total length of junctional interface (perimeter) per unit area (*I,* $p<0.0000038$). The amount of ZO-1 protein in the RPE fraction from TG retina was measured by western blotting (*J*) (5WT, 5TG retinas blotted), densitometric

scanning revealed a significant reduction in the amount of ZO-1 protein in the TG RPE fractions (*K*, p<0.001). RPE65 (*L*) and MerTK (*N*) protein levels in the RPE fractions were also measured by western blotting (4WT, 6TG retinas blotted), densitometric scanning revealed a significant reduction in the amount of both RPE65 protein (M, p<0.009) and MerTK (O, p<0.02) in the TG RPE fractions. (All error bars S.E.M., ** indicates p<0.001). Scale bars are 20μm in B and 200μm in C, D.

Fig. 3. Ultrastructural changes in the RPE^{Cre}/DTA retina**.** Representative EM images are shown from wild type (*A*) and transgenic (*B*) retinas. Images from 6 different animals in each group were analysed, and measurements taken. The width of the RPE cell layer was measured across the whole of the retina in each animal. (*C*) The average RPE thickness was not significantly different between the WT and TG retinas. The total number of phagosomes per unit length of RPE was quantified (*D*) and the distribution of phagosomes within the RPE cell, apical or basal was analysed (*E*). Although total phagosome numbers were not significantly different, there was a change in the intracellular profile of phagosome distribution, which is shown by a significant difference (p < 0.036) (Student's t test, 1 tailed, unpaired) in the apical:basal phagosomes ratio. Semi-thin (0.5 μm) toluidene blue stained sections are shown from a wild type control retina (*F*) and from a mildly affected (*G*) and a severely affected transgenic (*H*). (All error bars S.E.M., * indicates p<0.05-0.019). Scale bars are 2 μm in *A* and *B*, and 50 μm in *H*.

Fig. 4. Rhodopsin quantification**.** Rhodopsin quantification was performed by retinal extraction and spectral analysis. (*A*) Represents the average amount of pigment extracted from the 2 eyes of RPE^{Cre}/DTA transgenic (n=5) and wild type (n=6) animals. There was no significant difference in the amount of pigment in the RPE^{Cre}/DTA and wild type mice (Student's t test). A representative spectrum from 1 eye is shown (*B*) pre (solid) and post (dashed) bleach. The

amount of pigment in each eye was calculated from the peak absorbance of the difference spectrum (*C*). (All error bars S.E.M.).

Fig. 5. Electrophysiological assessment of the RPE^{Cre}/DTA transgenic mice and WT control animals. Representative ERG traces are shown for scotopic (*A,B,C*) and photopic (*D,E,F*) responses from a wild type control animal (*A,D*) and two different transgenic animals (*B,E* and *C,F*) to illustrate the range of responses evoked from the transgenic animals. ERG was used to assess the responses of the neural retina to light flashes of increasing intensity under both scotopic and photopic conditions. Under scotopic conditions the TG animals (n = 12) displayed significantly reduced a wave (*G*) and b wave (*H*) amplitudes, $p < 0.011$ and $p < 0.005$ respectively, tested by performing an ANOVA with repeated measures (SPSS, GLM repeated measures) in comparison to WT control animals (n=11). Under photopic conditions the b wave (*I*) showed no significant difference in the transgenic animals in comparison to control responses. The initial slope of the scotopic a wave was measured over 5 ms (*J*) from the brightest flash, log intensity 1. The transgenic animals have a significantly reduced gradient in comparison to wild type $p < 0.00097$ (one-tailed Student's t test) (all error bars S.E.M., ** indicates $p<0.01$).

Figure 1

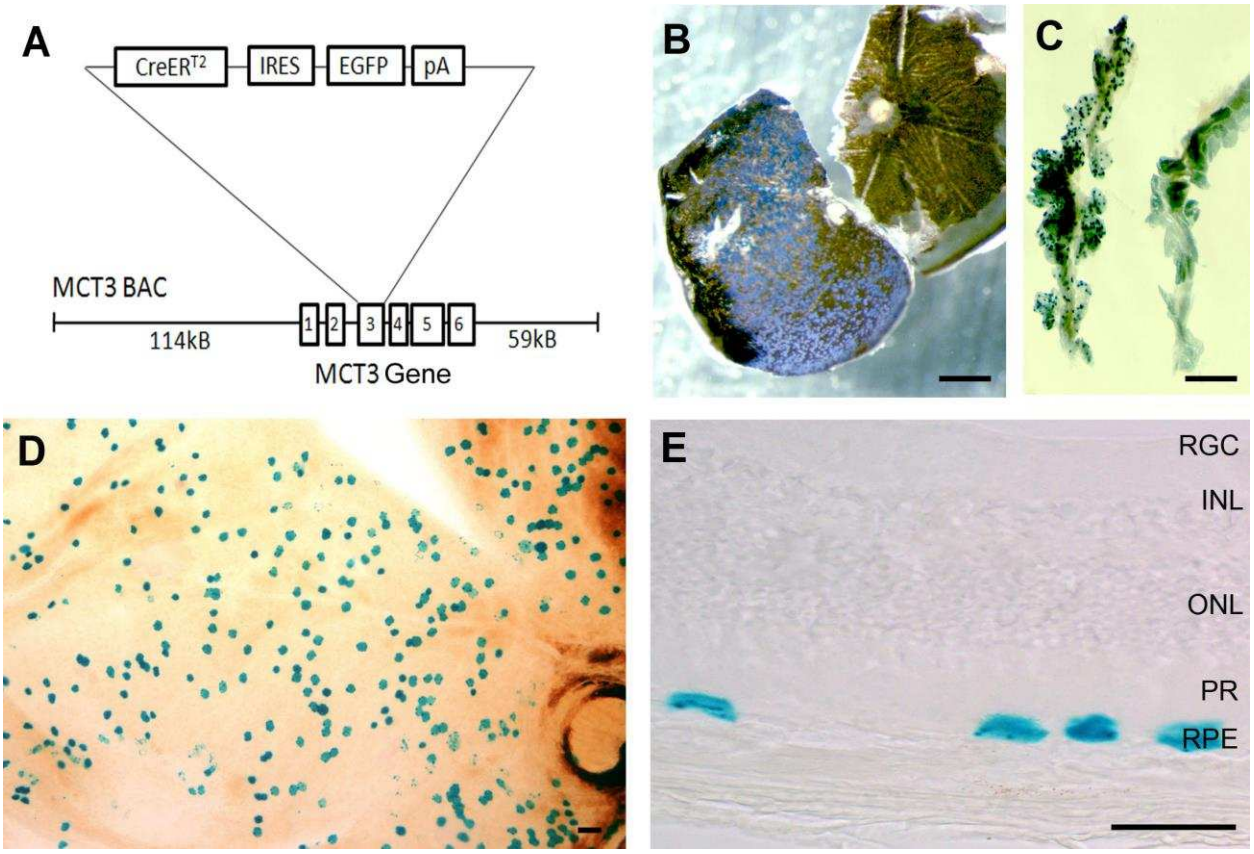
A
CreER^{T2}
IRES
EGFP
pA
MCT3 BAC
114kB
1
2
3
4
5
6
59kB
MCT3 Gene
B
C
D
E
RGC
INL
ONL
PR
RPE

Figure 2

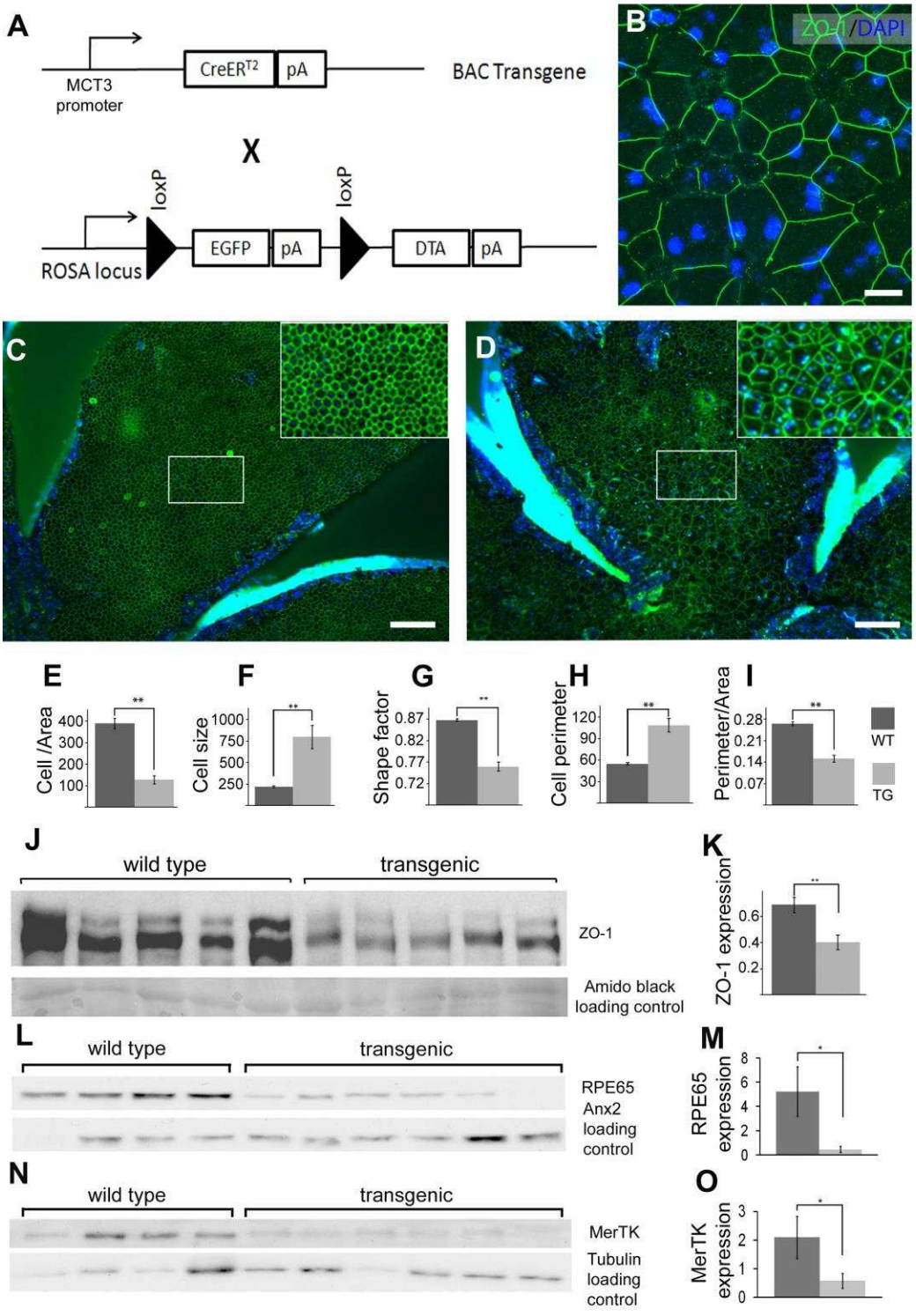
A
MCT3 promoter
CreER^{T2}
pA
BAC Transgene
X
loxP
loxP
ROSA locus
EGFP
pA
DTA
pA
B
ZO-1 /DAPI
C
D
E
Cell /Area
400
300
200
100
**
F
Cell size
1000
750
500
250
**
G
Shape factor
0.87
0.82
0.77
0.72
**
H
Cell perimeter
120
90
60
30
**
I
Perimeter/Area
0.28
0.21
0.14
0.07
**
WT
TG
J
wild type
transgenic
ZO-1
Amido black loading control
K
ZO-1 expression
0.6
0.4
0.2
**
L
wild type
transgenic
RPE65
Anx2 loading control
M
RPE65 expression
8
6
4
2
0
*
N
wild type
transgenic
MerTK
Tubulin loading control
O
MerTK expression
3
2
1
0
*

Figure 3

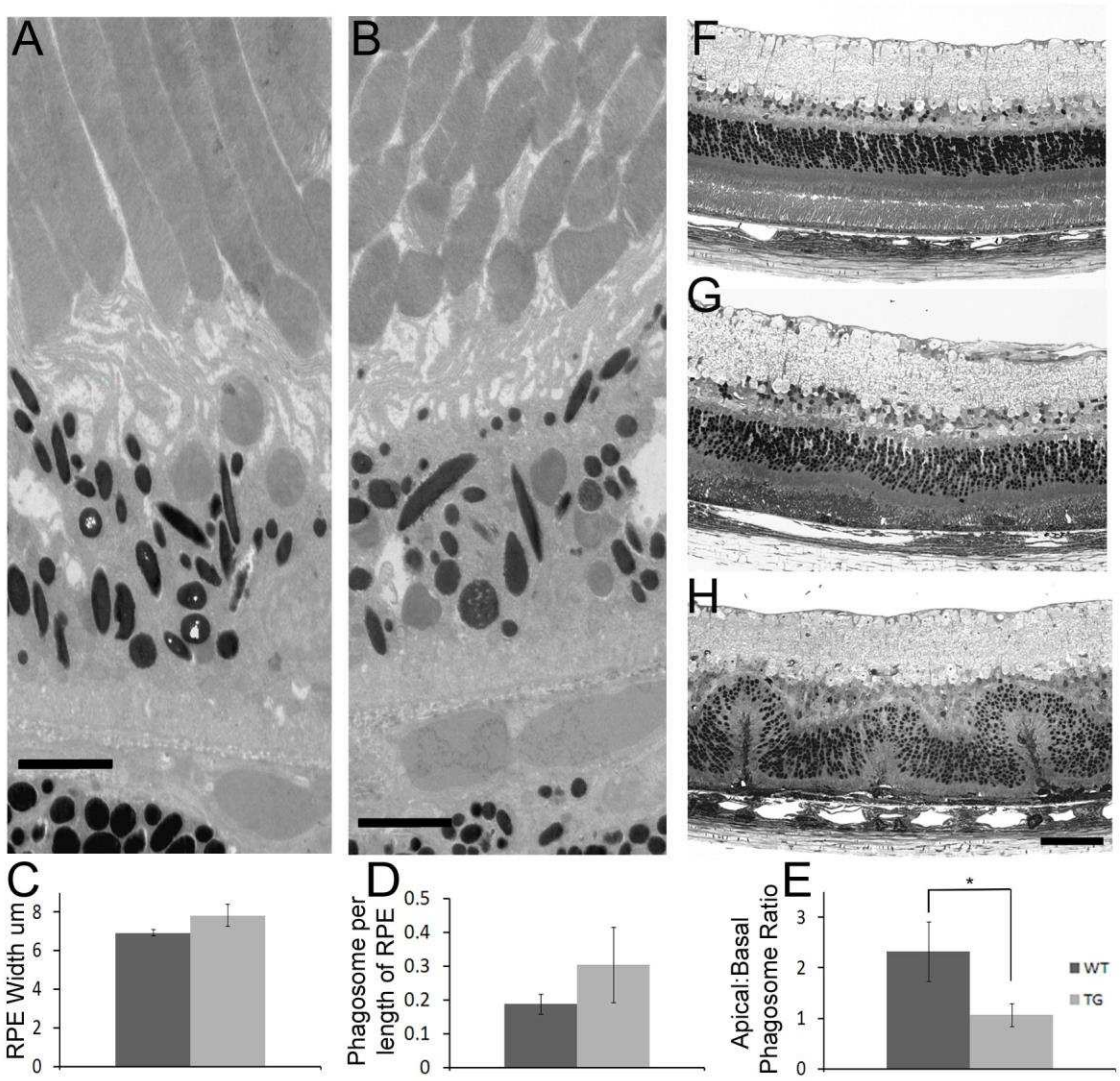
A
B
F
G
H
C
RPE Width um
0
2
4
6
8
D
Phagosome per length of RPE
0
0.1
0.2
0.3
0.4
0.5
E
Apical:Basal Phagosome Ratio
0
1
2
3
*
WT
TG

Figure 4

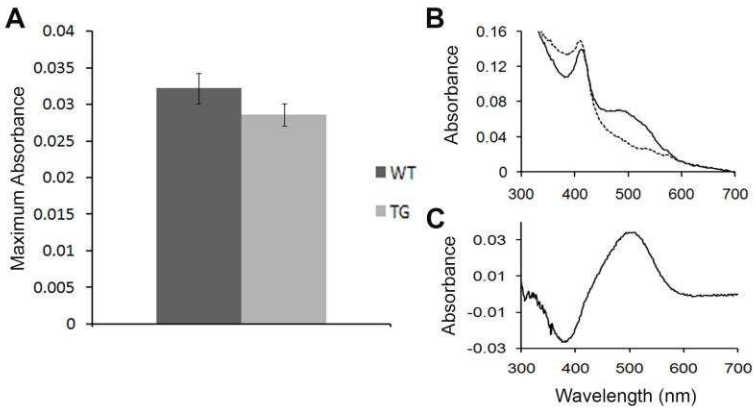
A
Maximum Absorbance
0.04
0.035
0.03
0.025
0.02
0.015
0.01
0.005
0
WT
TG
B
Absorbance
0.16
0.12
0.08
0.04
0
300
400
500
600
700
C
Absorbance
0.03
0.01
-0.01
-0.03
300
400
500
600
700
Wavelength (nm)

Figure 5

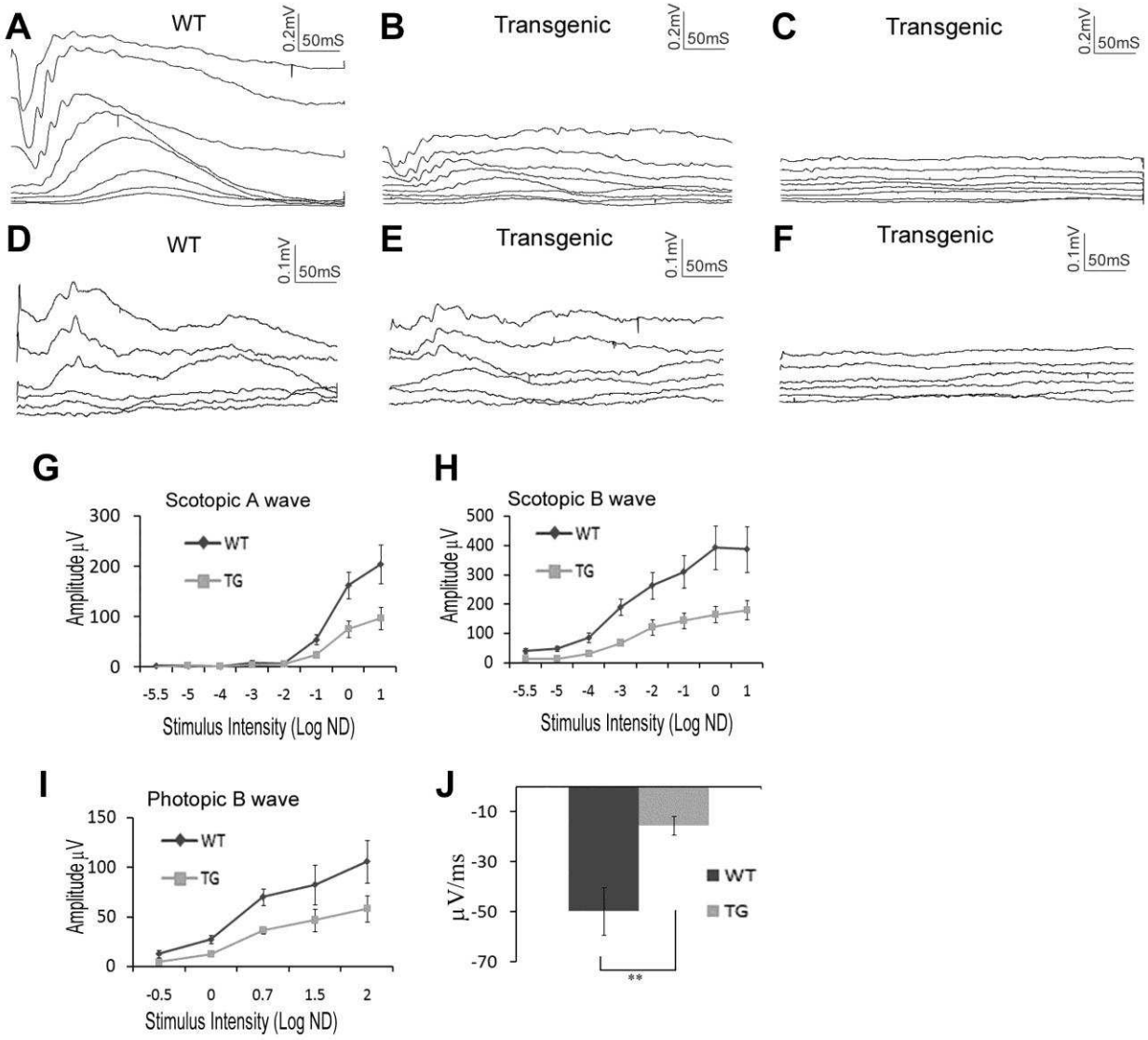
A
WT
0.2mV
50mS
B
Transgenic
0.2mV
50mS
C
Transgenic
0.2mV
50mS
D
WT
0.1mV
50mS
E
Transgenic
0.1mV
50mS
F
Transgenic
0.1mV
50mS
G
Scotopic A wave
Amplitude μV
300
200
100
0
WT
TG
-5.5 -5 -4 -3 -2 -1 0 1
Stimulus Intensity (Log ND)
H
Scotopic B wave
Amplitude μV
500
400
300
200
100
0
WT
TG
-5.5 -5 -4 -3 -2 -1 0 1
Stimulus Intensity (Log ND)
I
Photopic B wave
Amplitude μV
150
100
50
0
WT
TG
-0.5 0 0.7 1.5 2
Stimulus Intensity (Log ND)
J
μV/ms
-10
-30
-50
-70
WT
TG
**